Bull. Disas. Prev. Res. Inst., Kyoto Univ., Vol. 32. Part 1, No. 286, 1982

Characteristics of Sediment Motion for Respective Grain Sizes of Sand Mixtures

by Hiroji NAKAGAWA, Tetsuro TSUJIMOTO
and Susumu NAKANO

(Manuscript received December 23, 1981)

Abstract

In sediment transport of sand mixture, the characteristic quantities of sand motion are different for each grain size, and it follows that temporal and spatial changes of bed constitution must be caused thereby. Therefore, the characteristic quantities of sand motion for each grain size should be clarified in relation to bed constitution to describe sediment transport process and subsequent phenomena in alluvial beds composed of sand mixtures. At first, mechanical properties of rough bed composed of sand mixture are investigated in relation to grain size distribution, and particularly the statistical properties of relative height and angle of escape of exposed particles are inspected by a simulation method. Next, the so-called critical tractive force for each grain size, which is one of the most fundamental quantities, is here theoretically investigated. On its estimation, the equivalent sand roughness of mixed sand bed is necessary and a new model using the concept of equivalent size of non-uniform particulate materials is proposed. Moreover, the other characteristic quantities of sediment motion for each grain size are inspected based on a film analyzing method. These research projects must give important information to describe various kinds of alluvial phenomena observed in natural rivers of which beds are composed of widely distributed sands and gravels.

1. Introduction

In sediment transport of sand mixture, the difference of characteristic quantities for each grain size causes a change of bed constitution as well as the change of transport process itself. Such a complicated phenomenon cannot be explained by applying a sediment transport formula as an all-round expression, but the individual constituent elements of transport process must be investigated for each grain size in relation to bed constitution and the process as a whole must be described based on this relationship.

The most suggestive research for this problem is Egiazaroff's one,[1] where the critical tractive force for each grain size has been derived, and this has been applied to the sediment transport rate formulae by Hirano[2] and Ashida et al.[3] However, gradation properties of sand mixtures have not been sufficiently considered in Egiazaroff's model, and a mere substitution of the critical tractive

force for each grain size given by Egiazaroff's model to bed load transport formula in equilibrium condition cannot be appropriate because a non-equilibrium situation is inevitably caused in any transport process of sand mixtures. Therefore, more detailed treatment is necessary for this kind of problem.

In this paper, the characteristics of grain size distribution of a sand mixture are at first inspected, particularly the relation between the characteristics of bed surface constitution and grain size distribution of an entire mixture is inspected because individual sediment motion and subsequent bed changes can only depend upon the top layer of the sand bed. On the other hand, sediment transport process can be divided into the two sub-processes: incipient motion and travelling process of moving particles. The former can be represented by the so-called critical tractive force, and a physical model is derived under consideration of mechanical properties of sand mixtures. Furthermore, the estimation of sediment pick-up rate for each grain size, which is a better representation of incipient motion than the critical tractive force, is investigated based on this model. As it is difficult to make a physical model for travelling sub-process, it is mainly investigated based on experimentally obtained data. Namely, so-called constituent elements of bed load transport formulae are measured by a flume experiment and their characteristics are inspected from a viewpoint of mechanics of particle motion. These measurements are performed by a film-analyzing method using a 16 mm movie camera and a dynamic frame.

2. Mechnical Properties of Bed Composed of Sand Mixture

2.1 Fundamental consideration on grain size distribution

The properties of an entire mixture are usually represented by a weight basis distribution of grain size, which is obtained by a sieve analysis. The density function of this weight basis distribution of the entire mixture is to be expressed by $p(d)$. By the way, sediment motion and subsequent bed changes are limited to the region near the bed surface, and only the materials exposed at the bed surface are significant. In case of sand mixtures, grain size distribution of the exposed materials must be different from that of the entire mixture. Particularly, a number basis distribution of the exposed materials is significant for an analysis of individual sediment motion, and its density function is to be represented by $\hat{p}(d)$. Moreover, in case of the sampling of bed surface materials using grease, wax or spatula, the weight basis distribution of the exposed materials is adopted, and its density function is to be represented by $\tilde{p}(d)$. In any study on sediment mixtures, the above-mentioned three distributions are often used, and it is necessary to clarify the basic relations among them.

When $\hat{p}(d)$ is known, $\tilde{p}(d)$ can be calculated using the following equation, because a weight basis distribution is identical with a volume based one.

$$\tilde{p}(d) = \hat{p}(d)\, d^3 / \int_a^b \eta^3 p(\eta)\, d\eta \tag{1}$$

where a is the maximum diameter and b is the minimum one of the sand mixture. Inversely, the following equation is valid.

$$\hat{p}(d) = \{\tilde{p}(d)/d^3\} / \int_a^b \{\tilde{p}(\eta)/\eta^3\}\, d\eta \tag{2}$$

By the way, a sample of the thickness of one sand grain of exposed materials should be gathered. If, on the other hand, the gathering thickness of the sample becomes large enough, the sample would represent the entire mixture. When $\hat{p}(d)$ and the number of sampled exposed sand grains N are given, the number of exposed grains of which diameter is in the interval $[d, d+\Delta d]$ is $N\hat{p}(d)\Delta d$. If the sampling thickness is s and the gradation of the mixture is homogeneous in depth, the number of grains of this size-class involved in the sample is $N\hat{p}(d)\Delta d \cdot (s/A_1 d)$, where A_1 is one dimensional geometrical coefficient of sand. Hence, $p(d)$ can be calculated from $\hat{p}(d)$ as follows.

$$p(d) = N\hat{p}(d) \cdot (s/A_1 d) \cdot A_3 d^3 / \{(NsA_1/A_3) \int_a^b \eta^2 \hat{p}(\eta)\, d\eta\}$$

$$= d^2 \hat{p}(d) / \int_a^b \eta^2 p(\eta)\, d\eta \tag{3}$$

where A_3 is three-dimensional geometrical coefficient of sand. According to the above equation, $p(d)$ can be also regarded as the density function of the area occupied by the sand grains of diameter d. Hence, when $p(d)$ is known,

$$\hat{p}(d) = \{p(d)/d^2\} / \int_a^b \{p(\eta)/\eta^2\}\, d\eta \tag{4}$$

The mean diameters are defined for the above three distributions; $p(d)$, $\hat{p}(d)$ and $\tilde{p}(d)$, respectively:

$$d_m = \int_a^b \eta p(\eta)\, d\eta, \quad \hat{d}_m = \int_a^b \eta \hat{p}(\eta)\, d\eta, \quad \tilde{d}_m = \int_a^b \eta \tilde{p}(\eta)\, d\eta \tag{5}$$

These are the weight basis mean diameter of the entire mixture, the number basis and the weight basis mean diameters of the exposed materials, respectively. Similarly, several kinds of median diameters can be defined.

The above-mentioned relationships have been verified experimentally. In the experiments, three kinds of sand mixtures which were artificially prepared were used, and $p(d)$ was predetermined for each mixture. The sample mixtures were colored by six kinds of volatile ink in order to distinguish the individual classes of grain size from one another. Sand beds composed of these mixtures were carefully prepared and the bed constitutions were inspected by photo to obtain $\hat{p}(d)$. Moreover, the top layers of the test beds were carefully lifted off by a spatula, and sieve analyses of dried samples were done to get $\tilde{p}(d)$. $p(d)$,

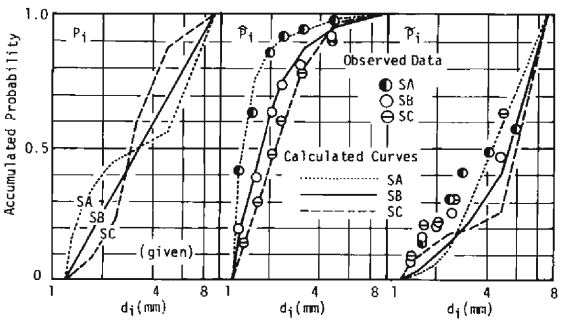

Fig. 1 Measured Grain Size Distributions.

$\hat{p}(d)$ and $\hat{p}(d)$ are shown in **Fig. 1** by accumulated probabilities, and they are compared with theoretically calculated curves. From this figure, it is recognized that $\hat{p}(d)$ can be measured by photo with good accuracy, and $p(d)$ and $\hat{p}(d)$ can be mutually converted. On the other hand, $\tilde{p}(d)$ can be measured by the lifting-off method with less accuracy because of the difficulty of this technique, and thus a direct sampling method of the exposed materials must be improved in future.

2.2 Some calculations for typical distributions

Grain size distribution of sand mixture is liable to show an asymmetric type, and a log-normal type is frequently adopted. In fact, most of the previous data in fields show the adaptability of a log-normal distribution.[4] Moreover, in case of log-normal distribution, theoretical calculation is easy. However, the range of sand diameter in this case is $(0, \infty)$ against the fact. The simplest case where the maximum and the minimum are finite is a "log-linear" type of distribution, of which distribution curve is linear on a semi-logarithmic paper. Here, these two types of distribution are inspected.

When the weight basis distribution of the entire mixture follows a log-normal one, $p(d)$ is expressed as follows:

$$p(\eta)\,d\eta = \frac{1}{\log \sigma_g \sqrt{2\pi}} \exp\left\{-\frac{(\log \eta - \log d_{50})^2}{2 \log^2 \sigma_g}\right\} d(\log \eta) \tag{6}$$

where

$$\log d_{50} = \int_0^\infty \log \eta\, p(\eta)\, d\eta; \quad \log \sigma_g = \left\{\int_0^\infty (\log \eta - \log d_{50})^2 p(\eta)\, d\eta\right\}^{1/2} \tag{7}$$

d_{50} is the geometric mean diameter, which is identical with the median diameter, and $\log \sigma_g$ is the geometric standard deviation. Moreover, σ_g is the log-standard geometric deviation, and

$$\sigma_g = \sqrt{d_{84}/d_{16}} = d_{84}/d_{50} = d_{50}/d_{16} \tag{8}$$

where d_k is the size for which $k\%$ of the entire materials are finer by weight. The calculations using Eqs. (4) and (1) show that $\hat{p}(d)$ and $\tilde{p}(d)$ become similar to Eq. (6). In other words, if a log-normal distribution is available, all distributions are also log-normal irrespectively of sample or basis, and the log-standard geometric deviation is invariant. Moreover, the above calculations give the following relations.

$$\ln(\hat{d}_{50}/d_{50}) = -2\ln^2\sigma_g \tag{9}$$

$$\ln(\tilde{d}_{50}/d_{50}) = \ln^2\sigma_g \tag{10}$$

where $\hat{d}_{50}$ and $\tilde{d}_{50}$ are number basis and weight basis median diameters of the exposed materials, respectively. Furthermore, using Eq. (5), some mean diameters are calculated, and

$$\ln(d_m/d_{50}) = (1/2)\ln^2\sigma_g \tag{11}$$

$$\ln(\hat{d}_m/d_{50}) = -(3/2)\ln^2\sigma_g \tag{12}$$

$$\ln(\tilde{d}_m/d_{50}) = (3/2)\ln^2\sigma_g \tag{13}$$

The relationships given by the above equations are illustrated in **Fig. 2**. The results of direct calculations based on Eqs. (1)$\sim$(5) are also plotted there.

When the weight basis distribution of the entire mixture follows a log-linear one, its distribution function $P(d)$ and its density function $p(d)$ are expressed by the following equations.

$$P(\zeta) = 0.5 + (0.34/\ln\sigma_g)\cdot\ln\zeta \tag{14}$$

$$p(\zeta) = (0.34/\ln\sigma_g)\cdot(1/\zeta) \tag{15}$$

where $\zeta \equiv d/d_{50}$, and $\sigma_g \equiv \sqrt{d_{84}/d_{16}}$ for convenience' sake. The limits of the distributing range, ζ_0 and ζ_1 are given by

$$\zeta_0 = \sigma_g^{-1.47}\ ;\quad \zeta_1 = \sigma_g^{1.47} \tag{16}$$

In this case, the weight basis mean diameter of the entire mixture is analytically calculated, and

$$d_m/d_{50} = (\sigma_g^{1.47} - \sigma_g^{-1.47})/2.94\ln\sigma_g \tag{17}$$

$p(\zeta)$ can be converted to $\hat{p}(\zeta)$, and $\hat{d}_m/d_{50}$ can be calculated also analytically.

$$p(\zeta) = \{1/(\sigma_g^{2.94} - \sigma_g^{-2.94})\}\cdot(1/\zeta^3) \tag{18}$$

$$\hat{d}_m/d_{50} = 2/(\sigma_g^{1.47} + \sigma_g^{-1.47}) \tag{19}$$

Moreover, $\hat{d}_{50}/d_{50}$ can be obtained by putting $\hat{p}(\zeta) = 0.5$, and

$$\hat{d}_{50}/d_{50} = \sqrt{2/(\sigma_g^{2.94} + \sigma_g^{-2.94})} \tag{20}$$

The relationships between σ_g and the characteristic diameters such as d_m, $\hat{d}_m$ and $\hat{d}_{50}$ are shown in **Fig. 3**, where some directly calculated values are also

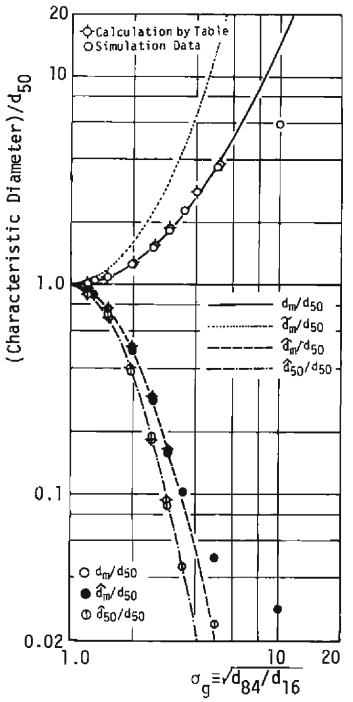

Fig. 2 Characteristic Diameters (Log-Normal Distribution).

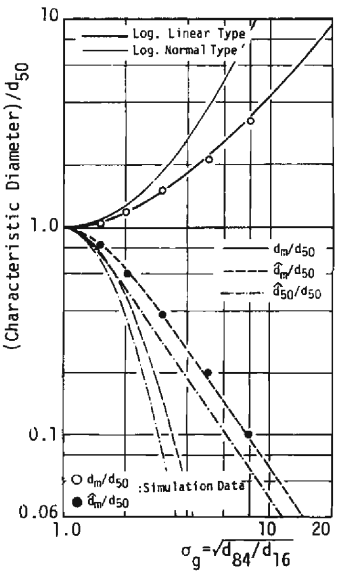

Fig. 3 Characteristic Diameters (Log-Linear Distrution).

plotted. These results are compared with the theoretical curves for log-normal type, and it is recognized that the changes of the characteristic quantities due to σ_g in case of log-linear type are more gradual than those in case of log-normal type. This tendency may depend upon whether the range of distribution is restricted or not.

Furthermore, some specialized distributions are inspected. At first, two kinds of distributions schematically illustrated in **Fig. 4(a)** are compared to each other: Sand W, widely distributed along both edges of distributing range of sand diameter, and Sand N, narrowly distributed along the both edges. The characteristic diameters calculated using the method similar to the above are shown in **Fig. 4(b)**. Next, the asymmetry of the distribution curve on a semi-logarithmic paper has been inspected. Namely, Sand G and Sand F, distribution curves of which are illustrated in **Fig. 4(c)**, are compared to each other. Here, apparent values of σ_g corresponding to the coarser part of sand mixture and the finer part, $\sigma_{gc} \equiv \sqrt{d_{84}/d_{50}}$ and $\sigma_{gf} \equiv \sqrt{d_{50}/d_{16}}$ $(\sigma_{gc} \cdot \sigma_{gf} = \sigma_g^2)$, and a parameter $\gamma_{cf} \equiv \sqrt{\sigma_{gc}/\sigma_{gf}}$ are introduced. The calculated results for the characteristic diameters are shown in **Fig. 4(d)**. From these analyses, it is recognized that the weight basis characteristics such as d_m are much influenced by the distribution properties of the coarser part, while the number basis characteristics such as $\hat{d}_m$ are by

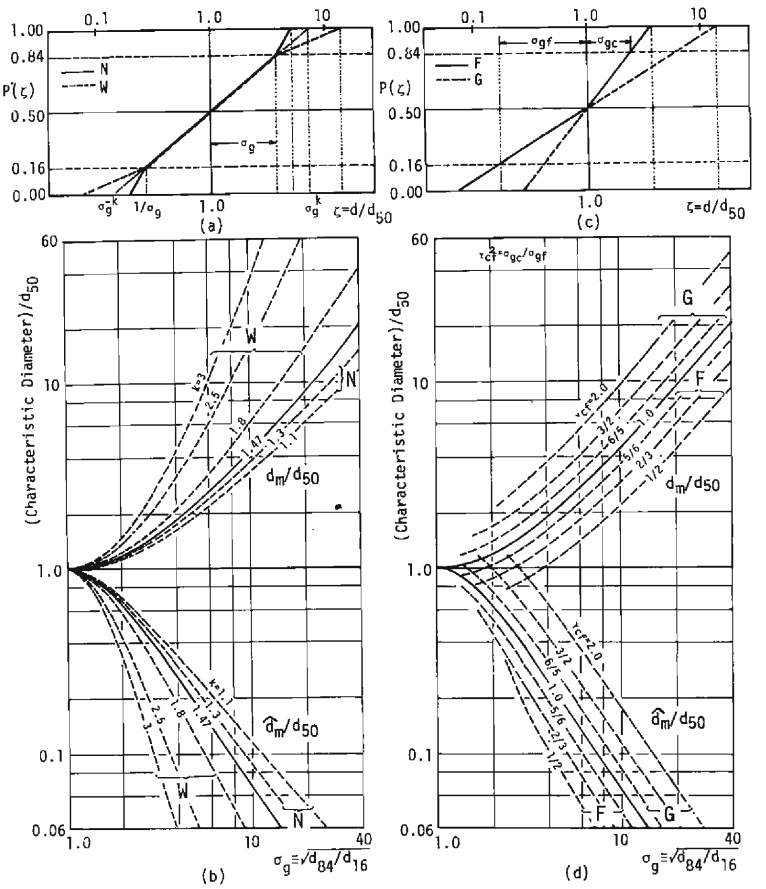

Fig. 4 Characteristic Diameters (Sands N, W and F, G).

those of the finer part.

2.3 The characteristics of rough bed composed of sand mixtures by simulation method

Though the most fundamental property of bed surface related to sediment motion is the number basis distribution of materials exposed at the bed surface, the relative position of individual exposed particle on the bed such as relative height and angle of escape must be clarified. However, an analytical treatment of this problem is difficult, and thus, the bed constitution is idealized and a numerical simulation is derived to inspect the fundamental properties as expressed by relative height and angle of escape.

For simplicity, an idealized two dimensional model is adopted here. The basic rough bed is considered at first, which is formed by non-uniform particles arranged for their centers to be connected in a straight line. It is assumed

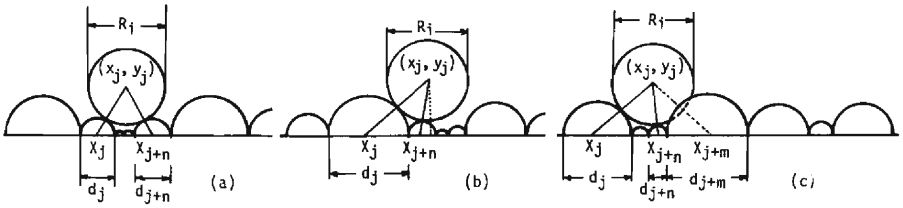

Fig. 5 Definition Sketch.

that the exposed particles are placed on this basic rough bed under stable states, as shown in **Fig. 5(a)**. The arrangement of non-uniform particles composing a basic rough bed and the patterns of stable states are probabilistic. These are here considered statistically using the number basis probability density function of exposed particles.

At first, $p(d)$ is given and this is converted to $\hat{p}(d)$ by using Eq. (3). Next, random numbers with mean unity following to $\hat{p}(d)$ are produced by converting the uniformly random numbers, and a hypothetical rough bed is determined by arranging the particles whose diameter are equal to the produced random numbers.

When a particle placed on the basic rough bed is put in contact with two particles composing the basic rough bed as shown in **Fig. 5(a)**, the coordinate of the center of the placed particle (x_j, y_j), and its angle of escape β_j can be expressed by

$$x_j = X_j + \sqrt{\left(\frac{D_j}{2}+\frac{R_i}{2}\right)^2 + (X_{j+n}-X_j)^2 - \left(\frac{R_i}{2}+\frac{D_{j+n}}{2}\right)^2}\Big/2(X_{j+n}-X_j) \tag{21}$$

$$y_j = \sqrt{\left(\frac{D_j}{2}+\frac{R_i}{2}\right)^2 - (x_j-X_j)^2} \tag{22}$$

$$\beta_j = \frac{\pi}{2} - \arcsin\{2y_j/(R_i+D_{j+n})\} \tag{23}$$

where X_j and X_{j+n} are x-coordinates of the centers of the two particles contacted with the placed particle, and D_j and D_{j+n} are the diameters of these two particles respectively; and R_i is the diameter of the placed particle. By Eqs. (21) and (22), (x_j, y_j) is calculated in succession from the condition $j=1$ and $n=1$. But it is necessary that the obtained point satisfies a condition that the three points $(X_j, 0)$, (x_j, y_j) and $(X_{j+n}, 0)$ can form a triangle. This condition is written as

$$x_j \geqq X_j + \sqrt{\left(\frac{D_j}{2}+\frac{R_i}{2}\right)^2 - \left(\frac{R_i}{2}\right)^2} \tag{24}$$

The points which do not satisfy the above condition must be rejected. Moreover, even if the above condition is satisfied, impossible states as shown in

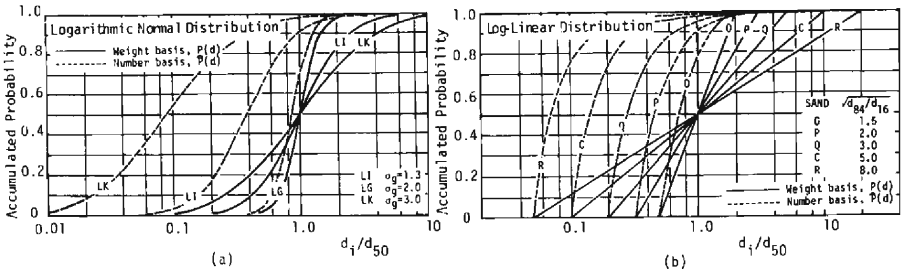

Fig. 6 Grain Size Distribution (Log-Nomral and Log-Linear Distributions).

Fig. 5(b), where the particle in the downstream side of the $(j+n)$-th particle obstructs a particle placed on the bed from contacting the j-th and the $(j+1)$-th particles, may be involved in the results. These must also be rejected. Its criterion is given by

$$\sqrt{(x_j-X_{j+n})^2+y_j^2}\geq R_i+D_{j+m} \quad (m\text{: arbitrary number}) \tag{25}$$

Lastly, even if the above conditions are satisfied, unstable states as shown in **Fig. 5(c)** may be involved in the results, and these must also be rejected. This criterion is given by

$$X_j<x_j<X_{j+n} \tag{26}$$

Under the above conditions, (x_j, y_j) and β_j $(j=1\sim2000)$ have been calculated for each R_i by computer, and their distributions have been inspected. The inspections have been carried out for several kinds of grain size distribution curves as shown in **Fig. 6**.

In **Fig. 7**, the average height of the center of exposed particle (the height from the level of the line connecting the centers of particles composing a basic

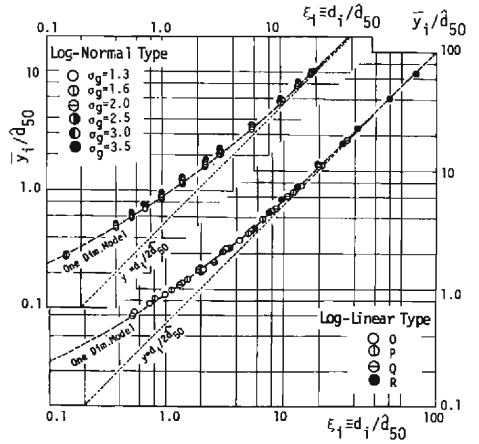

Fig. 7 Average Height of Particles Resting on Basic Rough Bed for Each Grain Size.

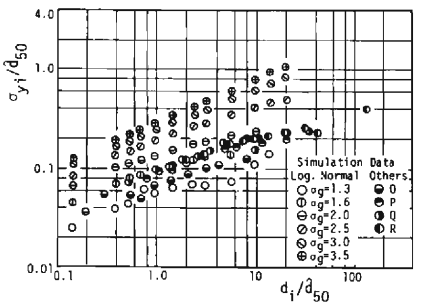

Fig. 8 Standard Deviation of Height of Exposed Particles for Each Grain Size.

rough bed) for each grain size, $\bar{y}_i$, is shown against $d_i/\hat{d}_{50}$. The characteristics of $\bar{y}_i$ are almost invariant among a log-normal type and a log-linear type, and the relationship between $\bar{y}_i$ and $d_i/\hat{d}_{50}$ is almost consistent with the broken line in the figure. This broken line indicates the theoretical result for a basic rough bed composed of uniform particles. In such an idealized case, the height of any exposed particle and the angle of escape for each grain size are deterministically given by the following equation.

$$\bar{y}_i/\hat{d}_{50}=\sqrt{\{(d_i/\hat{d}_{50})+1\}^2-1} \tag{27}$$

$$\bar{\beta}_{i0}=\arcsin\{\hat{d}_{50}/(\hat{d}_{50}+d_i)\} \tag{28}$$

On the other hand, the standard deviation of the height of exposed particle for each grain size, σ_{yi}, is shown in **Fig. 8**. When $d_i/\hat{d}_{50}=1.0$, the variation coefficient of $\{y_i\}$ is about 0.06～0.2, and the distribution of $\{y_i\}$ is comparatively narrow.

The average value of angle of escape for each grain size, $\bar{\beta}_i$, is shown in **Fig. 9**. According to this figure, the effect of σ_g in case of log-normal type is more appreciable than that in case of log-linear type. The broken line in this figure indicates Eq. (28), and this corresponds to the case $\sigma_g\to 1$. When all the particles have the same diameter, $\beta_0=\pi/6$, which is given by putting $d_i/\hat{d}_{50}=1$ in Eq. (28). Of course, it is the value for an idealized condition, and in fact the measured value for sand is larger than this because of the three dimensional effect. However, the ratio $\bar{\beta}_i/\beta_0$ may be significant, and the value of β_0 should be determined experimentally or theoretically after considering the three dimensional effect (see Appendix A).

The result for the variation coefficient of angle of escape for each grain size is shown in **Fig. 10**. According to this figure, the variation co-efficient of angle of escape for coarser sand is about 0.5～0.8, and the distribution of $\{\beta_i\}$ is more significant than that of $\{y_i\}$.

Furthermore, the correlation between $\{y_i\}$ and $\{\beta_i\}$ is also inspected. The correlation coefficient between $\{y_i\}$ and $\{\beta_i\}$, $\gamma_{y\beta i}$, has been calculated and the

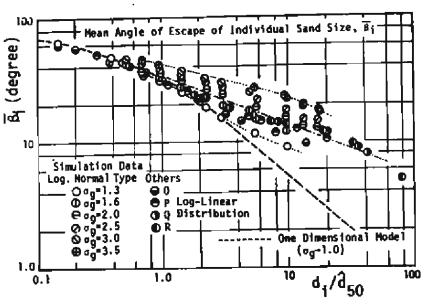

Fig. 9 Average Angle of Escape of Exposed Particles for Each Grain Size.

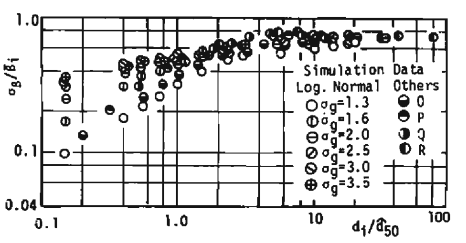

Fig. 10 Variation Coefficient of Angle of Escape for Each Grain Size.

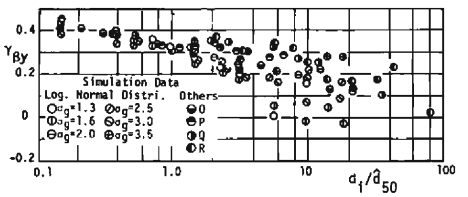

Fig. 11 Correlation Coefficient of Angle of Escape and Height of Exposed Particles for Each Grain Size.

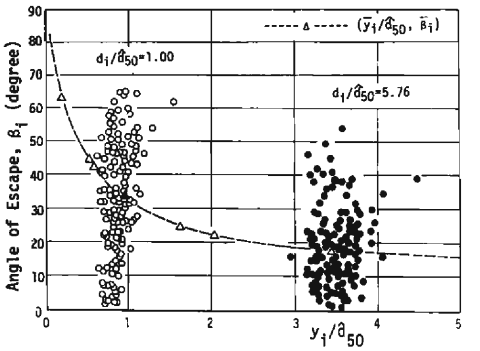

Fig. 12 Correlation between Angle of Escape and Height of Exposed Particles.

results are shown in **Fig. 11**. According to this figure, $0<\gamma_{y\beta i}<0.5$, and it can be concluded that the height and the angle of escape of individual exposed particles on bed surface for each grain size have a weakly positive correlation, though the average values, $\bar{y}_i$ and $\bar{\beta}_i$, have a negative correlation because $\bar{y}_i$ is larger and $\bar{\beta}_i$ is smaller for coarser sand. A part of data, which are the calculated results for the case of log-normal distribution, is shown in **Fig. 12**, and it is concluded that $\{y_i\}$ and $\{\beta_i\}$ can be regarded as being almost independently distributed. In **Fig. 12**, the correlation between $\bar{y}_i$ and $\bar{\beta}_i$ is also indicated by a broken line.

3. Theoretical Consideration on Critical Tractive Force for Each Grain Size

3.1 Criterion of incipient motion

It can be assumed that particles, except for much finer ones, are dislodged from a bed as rolling motion around the particle respectively contacting in downstream side in case of weak sediment transport under the condition of nearly critical tractive force. Considering the drag force D, the lift force L, and the submerged weight of sand W (see **Fig. 13**), the following equation is obtained for the critical condition for a particle of diameter d_i.

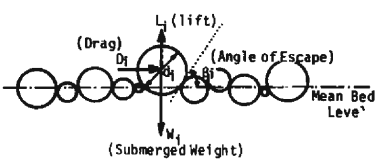

Fig. 13 Definition Sketch.

$$\frac{u_{bci}^2}{(\sigma/\rho-1)gd_i}=\frac{2A_s\cdot\sin\beta_i}{C_DA_2(k_1\sin\beta_i+\cos\beta_i)} \tag{29}$$

where C_D: drag coefficient, C_L: lift coefficient, σ: density of sand, ρ: density of fluid, g: gravity acceleration, u_b: local flow velocity near the sand particle, A_s: three-dimensional geometrical coefficient of sand, and β: angle of escape. Moreover, the subscripts, i and c represent the values corresponding to sand of diameter d_i and to the critical situation, respectively. In Eq. (29), it is assumed that C_D and C_L are constant irrespectively of sand diameter, and k_1 represents the ratio of C_L to C_D. Applying the logarithmic law for flow velocity profile in case of hydraulically rough regime, the dimensionless critical tractive force for each grain size, τ_{*ci}, can be obtained. Similarly, the dimensional critical tractive force for uniform sand τ_{*c0}, can be obtained. The obtained value of τ_{*c0} by this method does not necessarily coincide with that widely accepted because of additional effects due to turbulence and sheltering. However, the ratio of τ_{*ci} to τ_{*c0} validly indicates the effect of sand mixture. Hence, it is important to estimate this ratio, and the value of τ_{*c0} should be separately estimated by the previously established method for uniform sand. The ratio of τ_{*ci} to τ_{*c0} is written by

$$\frac{\tau_{*ci}}{\tau_{*c0}}=f_E(\beta_i)\cdot\left[\frac{\ln\{30.1(z_0/k_{s0})\}}{\ln\{30.1(z_i/k_s)\}}\right]^2 \tag{30}$$

where

$$f_E(\beta_i)=\frac{k_1\sin\beta_0+\cos\beta_0}{\sin\beta_0}\cdot\frac{\sin\beta_i}{k_1\sin\beta_i+\cos\beta_i} \tag{31}$$

z: the representative height of sand particle from the theoretical wall of velocity profile, k_s: the equivalent sand roughness, and the subscript 0 represents the value in case of uniform sand.

If it is assumed that $z=0.63d$, $\beta_i=\beta_0$ and $k_s=d_m$, Eq. (30) becomes almost identical with the well-known Egiazaroff's equation.[1] In Egiazaroff's original paper,[1] k_s is not always identical with d_m, but k_s is frequently assumed to be d_m for convenience' sake. In this case, the effect of sand mixture is represented only by $\zeta_i=d_i/d_m$, and it has been pointed out that the shape of grain size distribution cannot be considered.

3.2 Statistical situation of exposed particles for each grain size (Estimation of z_i and $f_E(\beta_i)$)

Here, the results obtained in the preceding chapter are applied, where the statistical properties of height of the center and angle of escape of a particle resting on a rough bed composed of non-uniform particles as shown in **Fig. 14(a)** have been investigated. Although the actual situations of river bed surface and exposed particles may be much different from this model, the critical trac-

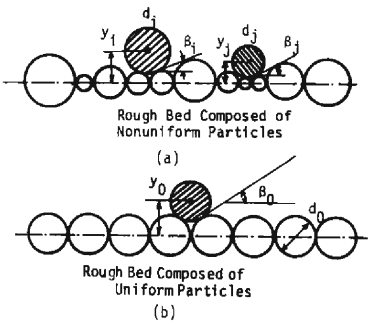

Fig. 14 Embedment Model.

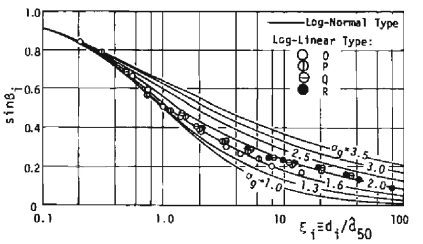

Fig. 15 The Relation between $\sin\beta_i$ and $\xi_i \equiv d_i/\hat{d}_{50}$.

tive force in case of uniform sand has also been investigated under an idealized condition as shown in **Fig. 14(b)** in almost all of the previous works. Hence, the information obtained from such a simplified model can be significant at least on estimating the ratio of the critical tractive force for each grain size of sand mixture to that of uniform sand.

According to the preceding chapter, the average height of particles resting on an idealized bed for each grain size is approximately expressed by the following equation irrespectively of grain size distribution as shown in **Fig. 7**.

$$\bar{y}_i/\hat{d}_{50} = \sqrt{\{(d_i/\hat{d}_{50})+1\}^2 - 1}/2 \tag{32}$$

By the way, z_i in Eq. (30) is the height of the center of the exposed particle from the theoretical wall of velocity profile, and then this may be slightly smaller than $\bar{y}_i$. However, the theoretical wall cannot be easily determined analytically, and z_i may be approximately estimated by the following equation.

$$z_i/\hat{d}_{50} = a\,(d_i/\hat{d}_{50})\,; \quad a = 0.5 \tag{33}$$

The relationship between $\sin\beta_i$ and $\xi_i \equiv d_i/\hat{d}_{50}$ is obtained as shown in **Fig. 15** based on **Fig. 9**. From this figure, the relationship between $\sin\beta_i$ and ξ_i varies with $\sigma_g \equiv \sqrt{d_{84}/d_{16}}$ in case of a log-normal type of size distribution, and in case of $\sigma_g \to 1$, $\sin\beta_i \to \{1/(1+\xi_i)\}$. Meanwhile in case of a log-linear type, the relation between $\sin\beta_i$ and ξ_i may not vary appreciably with respect to σ_g as mentioned in the preceding chapter.

As for the angle of escape for uniform sand, the one dimensional model gives that $\sin\beta_0 = 0.5$. Moreover, it is assumed that $k_1 = 0.85$ after the experimental result by Chepil,[5] and then, $f_E(\beta_i)$ is calculated as a function of $\sin\beta_i$. The relationship between $f_E(\beta_i)$ and ξ_i for a log-normal type of size distribution is shown in **Fig. 16.** In case of a log-linear type, the properties of $f_E(\beta_i)$ are almost similar to that for $\sigma_g \simeq 2$ of a log-normal type. As the relationship between $f_E(\beta_i)$ and ξ_i cannot be represented by any appropriate mathematical expression, **Fig. 16** should be used in the following.

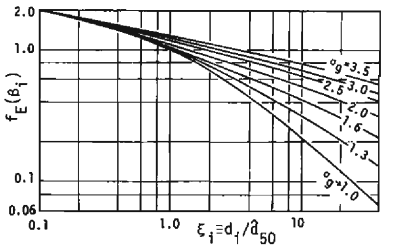

Fig. 16 The Relation between $f_E(\beta_i)$ and ξ_i.

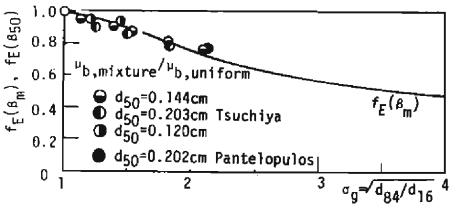

Fig. 17 Experimental Data for Frictional Angle of Sand Mixtures and Theoretical Curve of $f_E(\beta_m)$.

If a model, where sliding dislodgement is assumed as an incipient motion, is adopted, $f_E(\beta_i)$ corresponds to the ratio of the static friction coefficient for each grain size of sand mixture to that of uniform sand, μ_{bi}/μ_{b0}. The variation of the average static friction angle of sand mixtures due to the parameter σ_g was measured by Tsuchiya[4] for sand mixtures almost following log-normal type of size distribution. Such an averaged value may correspond to $f_E(\beta_m)$, where β_m is the average angle of escape for sands of d_m in mixture. Theoretical relationship between $f_E(\beta_m)$ and σ_g can be obtained by **Fig. 16** and the following equation.

$$\xi_m \equiv d_m/\hat{d}_{50} = \exp\{(5/2)\ln^2\sigma_g\} \tag{34}$$

The above equation is valid for a log-normal distribution and is obtained from Eqs. (9) and (11). The comparison between theoretical result and experimental data is shown in **Fig. 17**, and it shows a good agreement. $f_E(\beta_m)$ is a decreasing function of σ_g, and from this result it can be concluded that sand mixtures move more easily than uniform sand at least from the gravitational or frictional aspect.

3.3 Equivalent sand roughness of a bed composed of sand mixture

When the flow over a rough bed is represented by the so-called logarithmic law, the equivalent sand roughness should be estimated. Its estimation, however, is difficult particularly in case of sand beds composed of sand mixtures. In the previous study, d_m, d_{65} and others were adopted as k_s for convenience' sake without any physical background. Then, using the concept of "equivalent size of sand mixture", a physical model to determine k_s is proposed.[6]

Now, the flow properties as expressed by velocity profile over a mixed sand bed is to be equivalent to that over a uniform sand bed of diameter d_e. Then, tractive forces acting on both beds per unit area must be identified. Hence, the following equation must be valid.

$$\frac{\varepsilon_0}{2} C_D \rho u_{b0}^2 A_2 d_e^2 \cdot \frac{1}{A_2 d_e^2} = \sum \frac{\varepsilon_i}{2} C_D \rho u_{bi}^2 A_2 d_i^2 \cdot \frac{p_i}{A_2 d_i^2} \tag{35}$$

where p_i is relative frequency of particles of d_i by weight basis in an entire sand mixture, and ε is the so-called sheltering coefficient. It is assumed that ε_i is constant irrespectively of sand diameter and is equal to ε_0. Applying the logarithmic law for flow velocity profile in case of hydraulically rough regime, the following equation is obtained because the friction velocity is common for both beds.

$$\ln^2(30.1a/\alpha) = \sum[\ln^2(30.1a\eta_i/\alpha\eta_e)\cdot p_i] \tag{36}$$

where $k_s=\alpha d_e$, $\eta_i=d_i/d_{50}$, $\eta_e=d_e/d_{50}$, and α is a correction factor because k_s is not necessarily equal to grain size even in case of uniform sand. Here, the logarithmic law is significant only when

$$d_i > (\alpha d_e/30.1a) \tag{37}$$

Hence, it is assumed here that the acting forces in the direction tangential to the bed upon the particles finer than $(\alpha d_e/30.1a)$ must be zero. Rewriting the right hand side of Eq. (36) by continuous size distribution $p(\eta)$, the following equation with respect to η_e is obtained.

$$A(\eta_e)\ln^2\eta_e - 2B(\eta_e)\ln\eta_e + C(\eta_e) = 0 \tag{38}$$

where

$$\left.\begin{aligned} A(\eta_e) &= 1-P(\alpha\eta/30.1a)\\ B(\eta_e) &= \{1-P(\alpha\eta_e/30.1a)\}\ln(30.1/\alpha)+E'[\ln\eta]\\ C(\eta_e) &= 2\{\ln(30.1a/\alpha)\}\cdot E'[\ln\eta]+E'[\ln^2\eta]-P(\alpha\eta_e/30.1a)\cdot\ln^2(30.1a/\alpha)\end{aligned}\right\} \tag{39}$$

$$P(x) = \int_0^x p(\eta)\,d\eta \tag{40}$$

$$\left.\begin{aligned} E'[x] &= \int_{\alpha\eta_e/30.1a}^{\infty} x p(\eta)\,d\eta = E[x] - \int_0^{\alpha\eta_e/30.1a} x p(\eta)\,d\eta\\ E[x] &= \int_0^{\infty} x p(\eta)\,d\eta\end{aligned}\right\} \tag{41}$$

Though Eq. (38) is difficult to solve analytically, the first approximation of its solution can be easily obtained, where the condition given by Eq. (37) is removed, as follows.

$$\ln\eta_{e0} = \ln(30.1a/\alpha) + E[\ln\eta] - \sqrt{\ln^2(30.1a/\alpha) - \ln(30.1a/\alpha)\,E[\ln\eta] - Var[\ln\eta]} \tag{42}$$

where

$$Var[x] = E[x^2] - \{E[x]\}^2 \tag{43}$$

If the distributing range of grain size is narrow enough, the above approximation is effective. When a log-normal distribution is adopted,

$$\ln \eta_{e0} = \ln (30.1a/\alpha) - \sqrt{\ln^2 (30.1a/\alpha) - \ln^2 \sigma_g} \tag{44}$$

On the other hand, when $p(\eta)$ follows a log-linear type,

$$\ln \eta_{e0} = \ln (30.1a/\alpha) - \sqrt{\ln^2 (30.1a/\alpha) - 0.72 \ln^2 \sigma_g} \tag{45}$$

By the way, the higher order approximation of the solution of Eq. (38) can be obtained by the following method, in succession. When the j-th approximation, $\eta_{e,j}$, is known, the $(j+1)$-th approximation, $\eta_{e,j+1}$, is a solution of the following equation.

$$A(\eta_{e,j}) \ln^2 \eta_{e,j+1} - 2B(\eta_{e,j}) \ln \eta_{e,j+1} + C(\eta_{e,j}) = 0 \tag{46}$$

Therefore,

$$\eta_{e,j+1} = B(\eta_{e,j}) - \sqrt{B^2(\eta_{e,j}) - A(\eta_{e,j}) \cdot C(\eta_{e,j})} \tag{47}$$

The calculated results for η_e and η_{e0} are shown in **Fig. 18** by solid and dotted lines respectively, and $d_m/d_{50}(\equiv\eta_m)$ and d_{65}/d_{50}, which have been almost identified with k_s/d_{50} to date, are also shown in this figure. On the calculation to obtain this figure, it has been assumed that $a=0.5$ and $\alpha=1.0$. Comparing the present estimation of k_s with the experimental data,[7),8)] the scatterings of experimental data are so appreciable that one cannot conclude which estimation is good, but the present estimation is at least more reasonable than those adopted previously. Moreover, the idea mentioned here to estimate the equivalent sand roughness is so general that it can be applied to a kind of artificial roughness (see Appendix B).

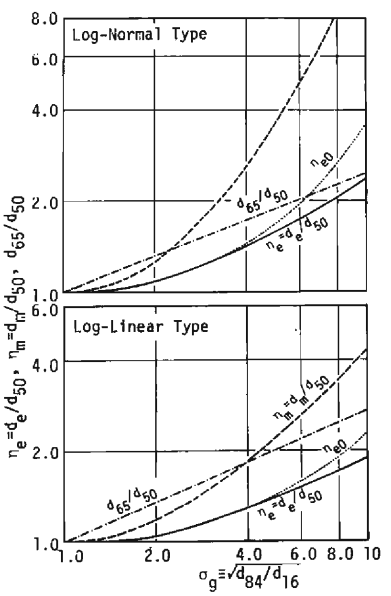

Fig. 18 The Calculated Results of η_{e0} and η_0.

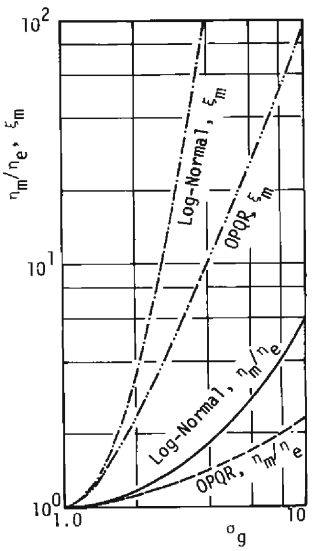

Fig. 19 $\eta_m/\eta_e\xi_m\sigma_g\equiv\sqrt{d_{84}/d_{16}}$.

3.4 Critical tractive force for each grain size of sand mixture

According to the above arguments, the critical tractive force for each grain size of sand mixture is obtained based on the following equation.

$$\tau_{*ci}/\tau_{*c0}=f_E(\beta_i)\cdot[\ln 15.05/\ln\{15.05(\eta_m/\eta_e)\zeta_i\}]^2 \qquad (48)$$

The above equation is written for the case that $a=0.5$ and $\alpha=1.0$. On calculation of Eq. (48), $f_E(\beta_i)$ is given by **Fig. 16**, and η_e by **Fig. 18**. Moreover, as for η_m and ξ_m, which is necessary to convert ξ_i in **Fig. 16** to ζ_i, and the variation of η_m/η_e and ξ_m against $\sigma_g\equiv\sqrt{d_{84}/d_{16}}$ are shown in **Fig. 19** for a log-normal and a log-linear (OPQR) types of grain size distribution.

Based on the above results, **Fig. 20** is obtained for a log-normal distribu-

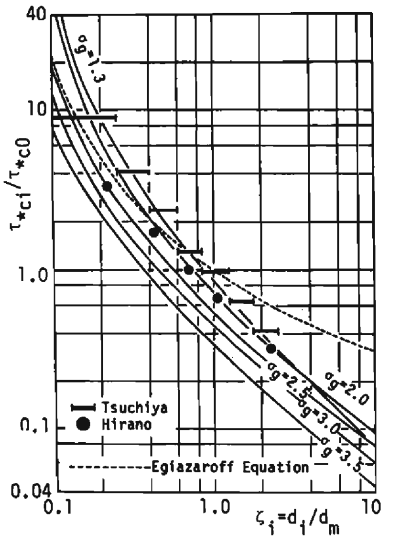

Fig. 20 The Ratio of Dimensionless Critical Tractive Force for Each Grain Size of Sand Mixture to That for Uniform Sand.

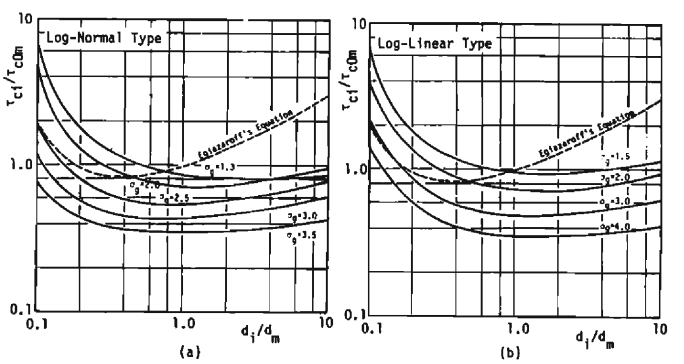

Fig. 21 The Ratio of Critical Tractive Force for Each Grain Size of Sand Mixture to That for Uniform Sand of Which Diameter is Equal to d_m.

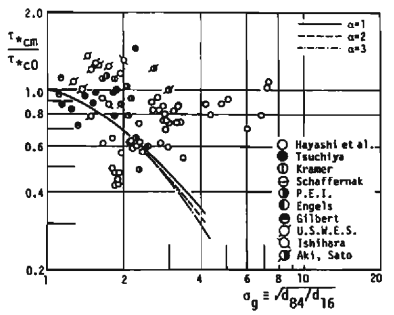

Fig. 22 Experimental Data for τ_{*cm}/τ_{*c0}.

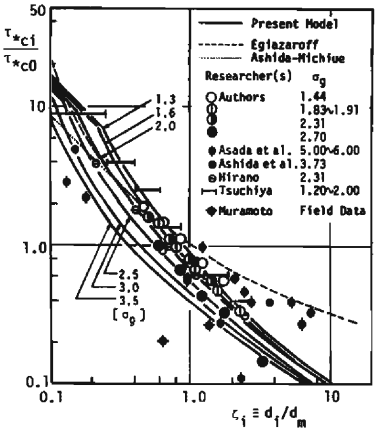

Fig. 23 The Ratio of τ_{*ci} to τ_{*c0}.

tion, and the experimental results rearranged from the data by Tsuchiya[4] and Hirano[2] are also shown. The theoretical result and the experimental data show good agreement. Particularly, the present model gives a better estimation for coarser sands than Egiazaroff's equation.[1]

Additionally, Eq. (48) can be rewritten in another version. Namely, it is $\tau_{ci}/\tau_{c0m}(=(\tau_{*ci}/\tau_{*c0})\zeta_i)$, and the calculated curve is shown in **Fig. 21**, where τ_{ci} is the critical tractive force for sand d_i in sand mixture and τ_{c0m} is that for uniform sand whose diameter is equal to d_m. According to **Fig. 20** and **21**, the present model can explain the difference of the critical tractive force for each grain size due to the difference of grain size distribution, and particles of d_m in sand mixture are easier to be dislodged than uniform sand which has diameter d_m, if the present model is applied. The experimental data collected by Tsuchiya[4] and Hayashi et al.[9] are shown in **Fig. 22**, and the fact explained above is certified roughly. Although in the present model only particles resting on the rough bed have been considered as done in almost all of the previous models for uniform sand, the bed constitution cannot always be such an idealized one and it must change during sediment transportation. Therefore, the present model cannot be universally applied, and the actual sand bed condition and its change by sediment transport should be carefully investigated in future, though the present model suggests a favorable approach to this kind of problem.

Another problem is concerned with incipient motion of much finer particles. These particles existing with coarser particles may be lifted up by turbulence strongly distorted by coarser sands. By considering this effect and using a simplified model for pressure fluctuation,[8] **Fig. 23** has been obtained. The result of this model is somewhat similar to the modification of Egiazaroff's equation by Ashida and Michiue.[3] However, it involves many ambiguous assumptions and it should be further improved in future. Additionally, some experimental data of critical tractive force for each grain size[2),3),4),10),11)] are also plotted in **Fig. 23.**

4. Experimental Study on Characteristics of Sediment Motion for Each Grain Size of Sand Mixture

In order to solve the sediment transport problem of sand mixtures reasonably, it is necessary to clarify the characteristic quantities of sand motion for each grain size. Therefore, the consistuent elements of bed load transport process are experimentally investigated for each grain size.

Experiments were conducted in a tilting flume 9m long and 33 cm wide. Five kinds of sand mixtures, grain size distributions of which are shown in **Fig. 24,** were prepared, and alluvial bed for each sand mixture was carefully laid in the experimental flume. The alluvial bed was 3 m long, and its upstream and downstream parts were made of fixed rough beds in order to keep the same hydraulic roughness throughout the flume.

Over the alluvial part of the experimental flume, a movie camera was set to make a film of the alluvial bed and the sediment motion on it. The number of frames of cinefilm per second was about 37～38. The precise value was obtained by taking pictures of a stop-watch for each experimental run. The pictured area on the alluvial bed was about 15 cm square. The pictured films were analyzed by a dynamic frame (a film motion analyzer) and a sonic digitizer

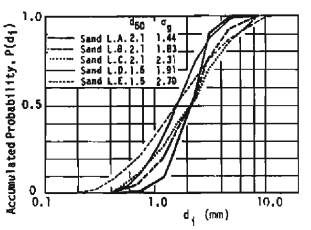

Fig. 24 Grain Size Distributions of Sand Mixtures Used in Experiments.

Table 1 Experimental Conditions.

RUN	h (cm)	U (cm/sec)	Fr	I_e	R_b (cm)	u_* (cm/sec)	u_*d_m/ν	τ_{*m}	d_{60} (cm)	d_m (cm)	σ_g
LA-1	7.27	46.5	0.55	0.0028	6.12	4.10	92	0.0462	0.210	0.225	1.44
LA-2	6.57	44.8	0.56	0.0033	5.70	4.29	97	0.0506	0.210	0.225	1.44
LA-3	7.11	47.0	0.56	0.0033	6.10	4.44	100	0.0542	0.210	0.225	1.44
LB-1	5.52	41.9	0.57	0.0033	4.86	3.96	100	0.0385	0.210	0.252	1.83
LB-2	6.41	45.9	0.58	0.0033	5.53	4.23	107	0.0439	0.210	0.252	1.83
LB-3	6.84	48.8	0.60	0.0033	5.81	4.34	109	0.0462	0.210	0.252	1.83
LB-4	8.56	55.8	0.61	0.0033	6.99	4.75	120	0.0554	0.210	0.252	1.83
LC-1	6.99	48.1	0.58	0.0033	5.96	4.39	119	0.0438	0.210	0.272	2.31
LC-2	7.11	47.4	0.57	0.0033	6.09	4.44	121	0.0448	0.210	0.272	2.31
LC-3	8.44	58.1	0.64	0.0033	6.80	4.69	128	0.0500	0.210	0.272	2.31
LC-4	5.01	43.7	0.30	0.0033	4.39	3.77	103	0.0323	0.210	0.272	2.31
LC-5	6.10	47.9	0.38	0.0033	5.24	4.11	112	0.0384	0.210	0.272	2.31
LC-6	6.38	51.5	0.42	0.0033	5.37	4.17	113	0.0395	0.210	0.272	2.31
LD-1	6.36	48.3	0.61	0.0033	5.41	4.18	73	0.0617	0.150	0.175	1.91
LD-2	8.26	53.5	0.59	0.0033	6.84	4.70	82	0.0781	0.150	0.175	1.91
LD-3	9.99	56.7	0.57	0.0032	8.07	5.03	88	0.0894	0.150	0.175	1.91
LD-4	11.24	61.7	0.59	0.0033	8.94	5.35	94	0.1011	0.150	0.175	1.91
LD-5	8.93	69.4	0.74	0.0052	7.31	6.11	107	0.1319	0.150	0.175	1.91
LD-6	10.32	64.1	0.64	0.0050	8.61	6.50	114	0.1493	0.150	0.175	1.91
LE-1	6.20	49.9	0.64	0.0033	5.24	4.12	94	0.0460	0.150	0.228	2.70
LE-2	7.72	56.5	0.65	0.0033	6.28	4.51	103	0.0552	0.150	0.228	2.70
LE-3	9.56	59.0	0.61	0.0029	7.46	4.60	105	0.0574	0.150	0.228	2.70
LE-4	11.52	60.7	0.57	0.0033	9.11	5.43	124	0.0800	0.150	0.228	2.70
LE-5	9.46	65.0	0.68	0.0050	7.86	6.21	142	0.1046	0.150	0.228	2.70
LE-6	13.88	59.5	0.51	0.0050	11.83	7.61	174	0.1517	0.150	0.228	2.70

to obtain instantaneous positions of individual sand particles. Sand particles were colored by 5～8 kinds of volatile ink in order that individual classes of grain size could be easily distinguished from one another.

The experimental conditions are indicated in **Table 1**, where h: flow depth, U: mean flow velocity, Fr: Froude number, I_e: energy gradient of flow, R_b: hydraulic radius only due to bed roughness and ν: kinematic viscosity of water. The measurements were finished before an appreciable armor coat had been formed in the measuring section.

4.1 Sediment pick-up rate for each grain size

For uniform sand, a model to estimate the pick-up rate p_s was derived by the authors previously,[12] and an approximated formula is written as

$$p_{s*}\equiv p_s\sqrt{d/(\sigma/\rho-1)g}$$
$$=F_*k_2B_*C_*\{(k_1\sin\beta+\cos\beta)/\beta\}\cdot\tau_*\{1-(\tau_{*c}/\tau_*)\}^3 \tag{49}$$

where $B_*=(\sigma/\rho-1)/\{(\sigma/\rho+C_M)(1+k_*^2)\}$, $C_*=(A_2/2A_3)\cdot A_*^2\cdot C_D$, $A_*=u_b/u_*$, F_*k_2: an experimental constant, C_M: added mass coefficient of sand particle, k_*d: gyration radius for the gravity center of a sand particle and u_*: friction velocity. In case of spherical uniform sand,[12]

$$F_0\equiv F_*k_2B_*C_*\simeq 0.03 \tag{50}$$

And, the pick-up rate for each grain size of sand mixture may be expressed by

$$p_{s*i}\equiv p_{si}\sqrt{d_i/(\sigma/\rho-1)g}$$
$$=F_0(\sin\beta_i/\sin\beta_0)(\beta_0/\beta_i)\tau_{*c0}\cdot(\tau_{*i}/\tau_{*ci})\{1-\tau_{*ci}/\tau_{*i})\}^3 \tag{51}$$

where Eqs. (30) and (31) have been used. The validity of the above equation will be verified here experimentally.

By the film analysis, the relationship between the measured dimensionless pick-up rate p_{s*i} and the dimensionless bed shear stress τ_{*i} has been obtained for each grain size, and it is shown in **Fig. 25**. In this figure, the experimental

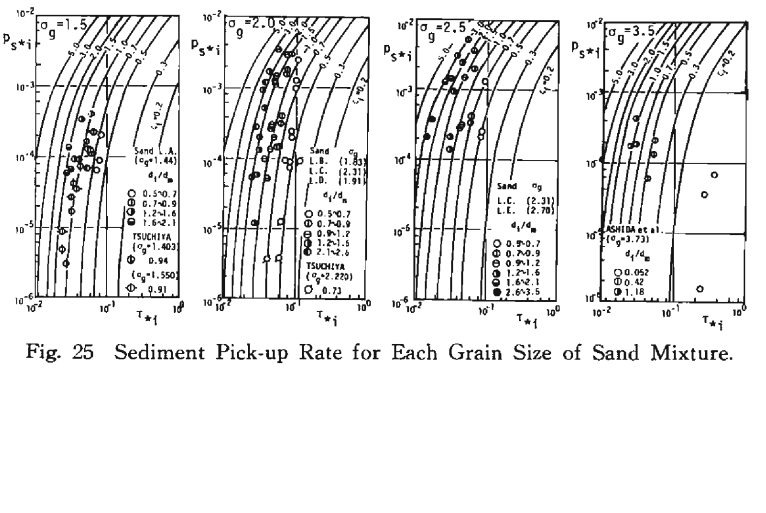

Fig. 25 Sediment Pick-up Rate for Each Grain Size of Sand Mixture.

data, which also involve the data rearranged from the experimental results obtained by Tsuchiya[4] and Ashida et al.,[3] are compared with the theoretical estimation based on the present model, where it is assumed that $\tau_{*c0}=0.035$.[12] According to this figure, the estimation of pick-up rate for each grain size based on the present model seems to be successful, though some scatterings of the experimental data are found.

4.2 Speed of moving particle for each grain size

In case of uniform sand, the average speed of bed load particles in motion can be comparatively well approximately by the equilibrium speed of sliding motion.[13] This does not necessarily support the conjecture that most of particles are sliding along the bed, but in fact some particles are sliding, others are rolling or in saltation, and the instantaneous speed of a particle appreciably varies mainly due to collisions with bed protrusions as clarified by the authors' research.[14] In case of sand mixture, if the above approximation is allowed for each grain size, the average speed of moving particles for each grain size $\overline{v}_{gi}$ can be given as follows.

$$\frac{\overline{v}_{gi}}{\sqrt{(\sigma/\rho-1)gd_i}}=\sqrt{\tau_{*i}}\left\{\frac{1}{\kappa}\ln\left(\frac{15.05d_i}{d_m}\cdot\frac{\eta_m}{\eta_e}\right)-\frac{2\mu A_3}{C_D A_2}\cdot\frac{1}{\sqrt{\tau_{*i}}}\right\} \tag{52}$$

where the logarithmic law for hydraulically rough flow is applied and κ is the Kármán constant. μ is the dynamic friction coefficient, which is assumed to be constant irrespectively of particle diameter, and the value of μ has been investigated in case of uniform sand to be about 0.35.[13] The above equation will be here experimentally inspected.

By 16 mm film analysis, instantaneous particle speed for each grain size has been evaluated from the travelling distance during about 0.03 sec. Since this quantity is clearly a probablistic one, about a hundred samples for each grain size have been extracted and statistically analyzed.

The results for the averaged speed of moving particles for each grain size obtained by a film analysis are compared with the theoretical estimation based on the above model in **Fig. 26**. Due to the narrow range of τ_{*i} in the experiments, the adaptability cannot be necessarily concluded but the tendency of the experimental data for each grain size can be comparatively well explained.

On the other hand, the experimental data for the variation coefficient of particle speed for each grain size, which is represented by α_{vi}, are shown in **Fig. 27**. Strictly speaking, α_{vi} seems to decrease with τ_{*i} for each grain size, and α_{vi} for finer particles seems larger for any value of τ_{*i}. Roughly speaking, the value of α_{vi} is about 0.3～0.6 and the difference of α_{vi} due to σ_g, τ_{*i} and d_i/d_m is not so appreciable. In other words, the normalized statistical distribution of particle speed is almost invariant though the mean value is different

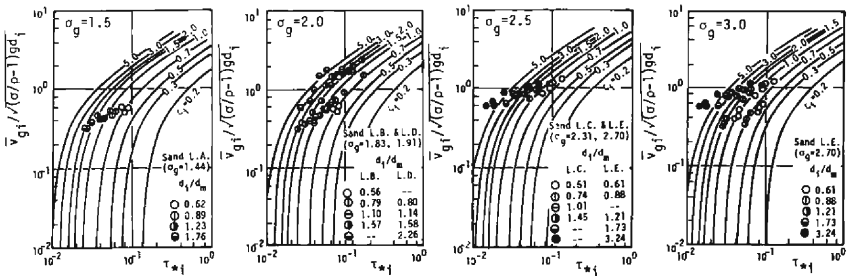

Fig. 26 Average Speed of Moving Particles for Each Grain Size of Sand Mixture.

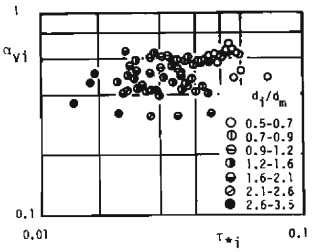

Fig. 27 Variation Coefficient of Particle Speed.

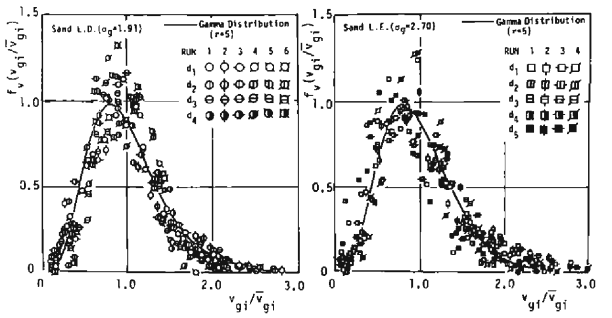

Fig. 28 Distribution of Particle Speed for Each Grain Size Mixture.

for each grain size. The above statement is supported by **Fig. 28**, where normalized probability density of particle speed for each grain size measured experimentally is shown. The solid line in this figure is the probability density function of gamma distribution, the shape parameter of which is 5, and it is consistent with the experimental results.

4.3 Number density of moving particles for each grain size

Though the concept of the number density of moving particles can be physically recognized, it is difficult to measure it by a film motion analysis because even a moving particle must be at rest instantaneously or in one frame of cinefilm. Therefore, the number density of moving particle, ν_{gi}, has been obtained from the transport rate, q_{Bi}, and the average speed of moving particles according to the following equation.

$$\nu_{gi} = q_{Bi}/\bar{v}_{gi}A_3 d_i^3 \tag{53}$$

As the fraction of area on a bed occupied by the i-th size class particles can be represented by p_i, the number of particles of diameter d_i exposed at the bed surface per unit area is $p_i A_2 d_i^2$ and the probability of motion for a sand of d_i is given by n_{*i}/p_i, where $n_{*i} \equiv \nu_{gi} A_2 d_i^2$. The relationship between n_{*i}/p_i and

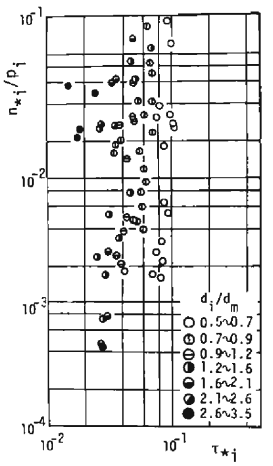

Fig. 29 The Relation between n_{*i}/p_i and τ_{*i}.

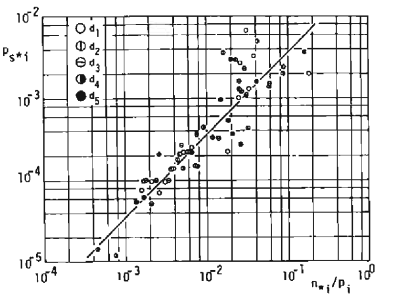

Fig. 30 The Relation between p_{s*i} and n_{*i}/p_i.

τ_{*i} is shown in **Fig. 29.** Comparing this figure with **Fig. 26**, the response of n_{*i} to τ_{*i} is more sensitive than that of $\overline{v}_{gi}$ to τ_{*i}, and then, it can be concluded that the increase of transport rate due to that of bed shear stress depends mainly upon that of the number density of moving particles. However, it is difficult to make a physical model to estimate the number density because the number density at any point cannot be always related to the bed shear stress at that point uniquely.

In case of equilibrium sediment transport, it is easily conjectured that n_* must be intimately related to p_{s*}. As the data of the present experiments are expected to be those for equilibrium conditions, the relationship between n_{*i}/p_i and p_{s*i} has been investigated based on them and it is shown in **Fig. 30.** According to this figure, the following linear relationship has been found out.

$$p_{s*i}=0.037n_{*i}/p_i \tag{54}$$

4.4 Step length and its distribution for each grain size

The estimation of step length is also difficult because the step length may be determined by probabilistic repetition of collisions with bed protrusions.[14),15)] Therefore, based on the above results clarified mainly by experiments the characteristics of the mean step length will be investigated here.

From the equations to give the transport rate in equilibrium, the folowing equation can be obtained.

$$n_{*i}/p_i=(\lambda_i/\overline{v}_{g*i})p_{s*i} \tag{55}$$

where $\overline{v}_{g*i}\equiv\overline{v}_{gi}/\sqrt{(\sigma/\rho-1)gd_i}$ and $\lambda_i\equiv\Lambda_i/d_i$. If Eq. (54), which has been experimentally obtained, is approved,

$$\lambda_i/\bar{v}_{g*i}=\text{const.}\simeq 1/0.037\simeq 27 \tag{56}$$

Meanwhile, the ratio of λ_i to $\bar{v}_{g*i}$ can be written as follows.

$$\lambda_i/\bar{v}_{g*i}=(\Lambda_i/\bar{v}_{gi})/\{d_i/\sqrt{(\sigma/\rho-1)gd_i}\} \tag{57}$$

The numerator of the right hand of the above equation represents the time for a sand particle to travel a distance Λ_i, and this can be called the "moving period" of a step. On the other hand, the denominator of the right hand of Eq. (57) represents the time for a grain to move a distance equal to its diameter by its terminal velocity. When these two characteristic times are represented by $T_m(\equiv\Lambda_i/\bar{v}_{gi})$ and $T_f(\equiv d_i/\sqrt{(\sigma/\rho-1)gd_i})$ respectively, Eq. (56) is rewritten as

$$T_m/T_f=27 \tag{58}$$

Though this result is interesting, its universal applicability has not been certified because the present experiments do not cover all the possible conditions.

By the way, the step length cannot be directly measured by a film analysis, because it is usually longer than the pictured region. Thus, most data for mean step length have been obtained by an indirect method as explained below: After $q_{B*i}(\equiv q_{Bi}/\sqrt{(\sigma/\rho-1)gd_i^3})$, p_{s*i} and p_i have been measured by a film analysis, λ_i has been indirectly obtained according to the following equation.

$$\lambda_i=(q_{B*i}/p_i)\cdot(A_2/A_3)\cdot(1/p_{s*i}) \tag{59}$$

Moreover, a part of the data have been obtained by direct measurements by eyes, where about a hundred samples for step length have been extracted for each grain size, and their mean has been calculated. These experimental data of mean step length for each grain size are compared with Eq. (56) in **Fig. 31**, and it is concluded that the mean step length for each grain size can be approximately estimated by Eqs. (56) and (52).

Sediment transport of sand mixture easily degenerates non-equilibrium, and not only the mean step length but also its distribution must play important roles in such a case. Hence, the distribution of step length for each grain size has

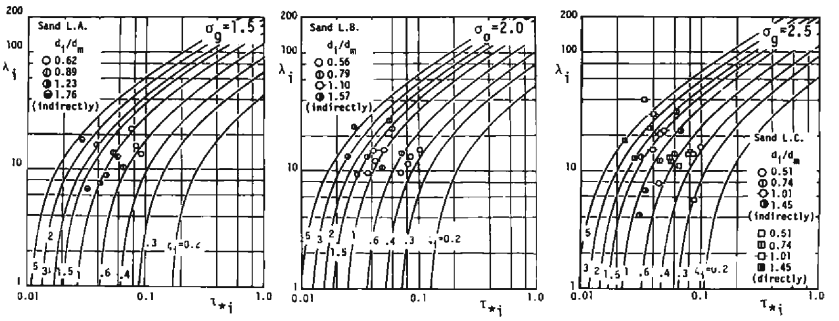

Fig. 31 Mean Step Length for Each Grain Size of Sand Mixture.

been investigated based on the experimental data obtained by direct measurements. The results are shown in **Fig. 32**, where $F_{Xi}(\xi)$ represents the distribution function of step length for each grain size, and it is concluded that the distribution of step length for each grain size of sand mixture can be regarded as an exponential one as well as that for uniform sand. Namely, its density function can be expressed by

$$f_{Xi}(\xi) = (1/\Lambda_i) \cdot \exp(-\xi/\Lambda_i) \qquad (60)$$

As known from **Fig. 31**, however, the mean step length is not always about a hundred times sand diameter as recognized in case of uniform sand, but the dimensionless mean step length for each grain size of sand mixture is generally somewhat smaller than that of uniform sand.

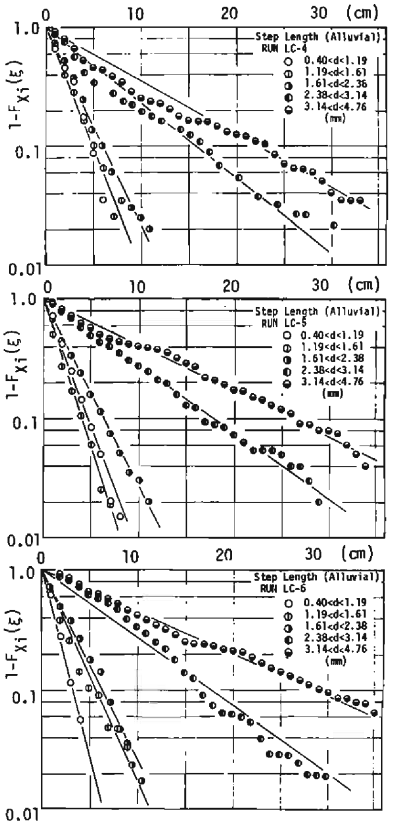

Fig. 32 Distribution of Step Length for Each Grain Size of Sand Mixture.

5. Conclusion

The results obtained in this study are summarized below:

In Chapter 2, the mechanical properties of mixed sand bed have been investigated. At first, the relationship between the distribution of materials exposed at bed surface, which is intimately related to bed load motion and subsequent change of bed constitution, and that of entire mixture has been inspected, and some examples have been shown. Furthermore, more concrete properties such as relative height of individual exposed particle and its angle of escape have been investigated by a derived simulation method.

In chapter 3, incipient motion of bed particles for each grain size has been theoretically investigated, and it has been clarified that the so-called critical tractive force for each grain size is determined by the statistical situation of exposed particle and the so-called equivalent sand roughness of mixed sand bed. Here, a new model to estimate the equivalent sand roughness has been reasonably derived using the concept of "equivalent size of non-uniform particles." The critical tractive force for each grain size obtained as a result of this chapter may give a better estimation than Egiazaroff's model particularly in case of the

coarser part of sand mixture. Moreover the present model can explain the effect of the shape of grain size distribution, which has not been considered to date.

In Chapter 4, experimental investigations on the characteristics of bed load motion for each grain size of sand mixture are explained. This chapter is based on the measurements of the constituent elements of bed load transport process for each grain size by a 16 mm film analysis. The sediment pick-up rate and the particle speed for each grain size can be well explained by physical models derived here. Furthermore, the number density of moving particles and the step length have been investigated and some instructive relationships have been experimentally obtained.

The information obtained in this study must be available for recognizing the internal structure of sediment transport process of sand mixtures, and they may be applied to analyses of some phenomena such as armoring process observed in alluvial streams composed of sand mixtures.

References

1) Egiazaroff, I. V.: Calculation of Non-Uniform Sediment Concentrations. Proc. ASCE, Journal of the Hydraulics Division, Vol. 91, HY4, pp. 225-247, 1965.
2) Hirano, M.: River-Bed Degradation with Armoring. Proc. JSCE, No. 195, pp. 55-65, 1971, (in Japanese).
3) Ashida, K. and M. Michiue: Study on Hydraulic Resistance and Bed-Load Transport Rate in Alluvial Streams. Proc. JSCE, No. 206, pp. 59-69, 1972, (in Japanese).
4) Tsuchiya, Y.: Study on Critical Tractive Force of Graded Sand Gravels. Annuals, Disaster Prevention Research Institute, Kyoto University, No. 6, pp. 228-253, 1953, (in Japanese).
5) Chepil, W. S.: The Use of Evenly Spaced Hemispheres to Evaluate Aerodynamic Forces on a Soil Surface. Trans. A.G.U., Vol. 39, No. pp. 397-404, 1958.
6) Nakagawa, H., T. Tsujimoto and S. Nakano: Roughness of Alluvial Bed Composed of Sand Mixtures and Incipient Motion of Individual Size-Class Sand. Proc. 25th Japanese Conference on Hydraulics, JSCE, pp. 67-72, 1981, (in Japanese).
7) Kikkawa, H., S. Fukuoka, T. Baba and F. Kawano: Study on Bed Load Transport Rate for Coarse Grains. Proc. 19th Japanese Conference on Hydraulics, JSCE, pp. 1-6, 1975, (in Japanese).
8) Nakano, S.: Fundamental Study on Sediment Transport of Sand Mixtures. Master Thesis, Department of Civil Engineering, Kyoto University, 1981, (in Japanese).
9) Hayashi, T., S. Ozaki and T. Ishibashi: Study on the Bed Load Transport of Sediment Mixture. Proc. 24th Japanese Conference on Hydraulics, JSCE, pp. 35-43, (in Japanese).
10) Asada, H. and H. Ishikawa: Study on Calculation of Sediment Discharge of Coarse Sand Bed. Technical Report, Technical Laboratory, Central Research Institute of Electric Power Industry, No. 68045, 1968 (in Japanese).
11) Muramoto, Y., Y. Kawata and A. Nunomura: Basic Study on the Bed Load in Gravel River. Annuals, Disaster Prevention Research Institute, Kyoto University, No. 20B-2, pp. 451-474, (in Japanese).
12) Nakagawa, H. and T. Tsujimoto: Study on Mechanism of Motion of Individual Sediment Particles. Proc. JSCE, No. 244, pp. 71-80, 1975, (in Japanese).
13) Nakagawa, H., T. Tsujimoto and H. Miyamoto: 16 mm Film Analysis of Characteristic Quantities of Bed Load Transport. Annuals, Disaster Prevention Research Institute, Kyoto

University, No. 21B-2, pp. 407-421, 1978, (in Japanese).
14) Nakagawa, H., T. Tsujimoto and Y. Hosokawa: Statistical Mechanics of Bed-Load Transportation with 16 mm Film Analysis of Behaviors of Individual Sediment Particles on a Flat Bed. Proc. 3rd International Symposium on Stochastic Hydraulics, Tokyo, Japan, IAHR-JSCE, Paper B-4, pp. 313-324, 1980.
15) Nakagawa, H., T. Tsujimoto, Y. Hosokawa and S. Murakami: Significance of Probabilistic Considerations in Dynamics of Bed Load Movement on Flat Bed. Proc. 24th Japanese Conference on Hydraulics, JSCE, pp. 27-34, 1980, (in Japanese).

Appendix A—Three-Dimensional Effect on Bed Constitution

Here, idealized three dimensional situations of bed constitutions are considered, and Eqs. (27) and (28) will be improved.

At first, two-dimensional arrangements of uniform size particles on a plane are considered as a basic rough bed, meanwhile in the section **2.3**, one dimensional arrangement has been considered. Then, the following patterns of arrangements of identical spherical particles can be considered as shown in **Fig. A**. Next, a particle of diameter ck is considered to be placed on the particles

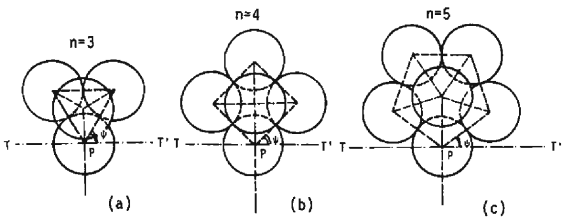

Fig. A Basic Patterns of Particles Arrangements (Plane View).

of diameter k arranged in the above patterns. The height of the center of the placed particle represented by y, and the other symbols are defined as shown in **Fig. B**. Consulting with **Fig. B**, the following can be derived:

$$y/k=\sqrt{(1+c)^2-4(A/k)^2},\quad A/k=1/(2\sin\psi),\quad \psi=\pi/n \qquad \text{(a)}$$

where n is the number of angles of a polygon which forms a basic pattern of arrangement ($n=3, 4, 5$), and ψ is an angle formed by a side of the polygon and the line T-T', which is perpendicular to the line P-O'. The point P is one of vertices of the polygon, and the point O' is the foot of the perpendicular from the center of the placed particle to the plane involving the polygon. When the placed particle moves along the plane DPO', the angle of escape becomes maximum. The point D represents the position of the center of the placed particle. In fact, however, the moving plane of the placed particle is not always on DPO' but it can revolve around an axis DO'. When the angle formed by the line P-O' and the intersecting line between the moving plane and the plane involving the polygon is to be represented by the symbol θ, the

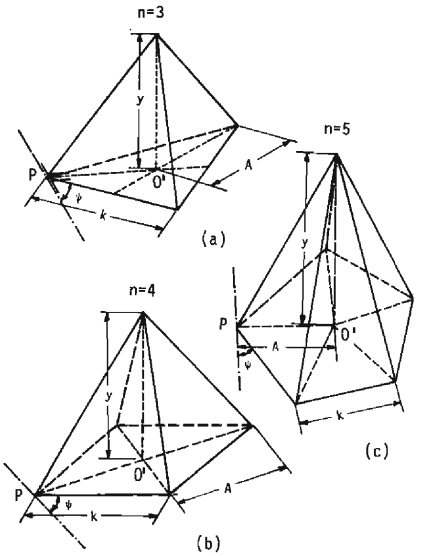

Fig. B Basic Patterns of Particles Arrangements.

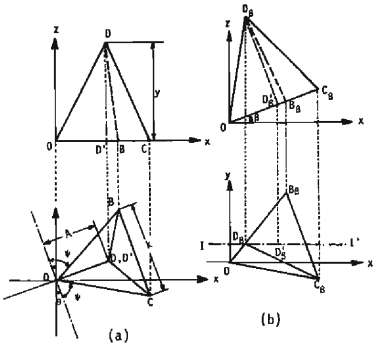

Fig. C Definition Sketch.

angle of escape β becomes a function of θ.

For simplicity, the case of $n=3$ will be considered as shown in **Fig. C(a)**. The moving plane of the placed particle is parallel with the x-z plane, and the angle of escape $\beta(\theta)$ is equal to the revolving angle of a tetrahedron D-OBC with respect to the y-axis in order to satisfy the condition where the trigon ODB is perpendicular to the x-y plane. The coordinates of the points D' and B are given as $D'(A\cos\theta,\ A\sin\theta,\ 0)$ and $B(k\sin(\psi-\theta),\ k\cos(\psi-\theta),\ 0)$, respectively. The point D' is the foot of the perpendicular from the point D to the plane OBC, and the situation where $0\leqq\theta<\psi$ is considered here. When the tetrahedron D-OBC revolves by an angle β around the y-axis, the points B, C, D and D' are to be translated to the points B_β, C_β, D_β and D_β', respectively (see **Fig. C(b)**). Namely, $D_\beta'(A\cos\theta\cos\beta,\ A\sin\theta,\ A\cos\theta\sin\beta)$, and $B_\beta(k\sin(\psi-\theta)\cos\beta,\ k\cos(\psi-\theta),\ k\cos(\psi-\theta)\sin\beta)$. When the coordinate of the point D is to be represented by $(\alpha,\ A\sin\theta,\ \gamma)$, the following relation should be valid.

$$(A\cos\theta\cos\beta-\alpha)^2+(A\cos\theta\sin\beta-\gamma)^2=y^2 \qquad \text{(b)}$$

Because the line O-D_β' is perpendicular to the line D_β-D_β',

$$\{(A\cos\theta\sin\beta-\gamma)/(A\cos\theta\cos\beta-\alpha)\}\cdot\tan\beta=-1 \qquad \text{(c)}$$

From Eqs. (b) and (c), the coordinate of the point D can be expressed by θ and β. Particularly,

$$\alpha=A\cos\theta\cos\beta-y\sin\beta \qquad \text{(d)}$$

If β is an angle of escape, the trigon ODB is perpendicular to the x-y plane

and then the orthogonal projection of the point D_β' to the x-y plane, that of the point B and the point O must be on a line. Hence, the following equation should be valid.

$$(A\cos\theta\cos\beta - y\sin\beta)/A\sin\theta = \sin(\psi-\theta)\cos\beta/\cos(\psi-\theta) \qquad \text{(e)}$$

Consequently, the following equation is obtained.

$$\beta(\theta) = \arctan[A\{\cos\theta - \tan(\psi-\theta)\sin\theta\}/y] \qquad \text{(f)}$$

In the above equation, y, A and ψ have already obtain in Eq. (a).

In **Fig. D**, the results for the height of the placed particles given by Eq. (a) are illustrated for the cases $n=3$, 4 and 5. The result of one dimensional model, for which Eq. (27) is obtained in the section **2.3** of this paper, is also indicated. Moreover, the relation expressed by Eq. (f) is illustrated in **Fig. E**, where the experimental results using glass beads are also shown. Particularly in case of uniform particles, the distribution of β after removing the condition for θ, which is assumed to be distributed at random, is shown as an accumulated probability for each value of n, in **Fig. F**. On the other hand, the experimental data for a glass bead on a rough bed composed of similar particles[a] are shown in **Fig. G**. In this experiment, the inclination of the rough bed was increased gradually and the probability that free particles on the bed start to move was measured. According to the experimental data, 30~40% for $20°<\beta<35°$; 40% for $35°<\beta<45°$; and 15% for $\beta>50°$, roughly. Meanwhile, the distribution of β obtained by the present model is limited in its range for each value of n; $20°<\beta<\simeq 35°$ for the case of $n=3$, $\simeq 35°<\beta<45°$ for the case of $n=4$ and $\simeq 52°<\beta<\simeq 58°$ for the case of $n=5$. Consequently, if the pattern of the arrangement of particles composing the rough bed is any of the idealized states, $n=3$, 4 or 5, locally, the probability of arrangement of n-gon, f_n, has been estimated as follows.

$$f_3\simeq 0.20, \quad f_4\simeq 0.65, \quad f_5\simeq 0.15 \qquad \text{(g)}$$

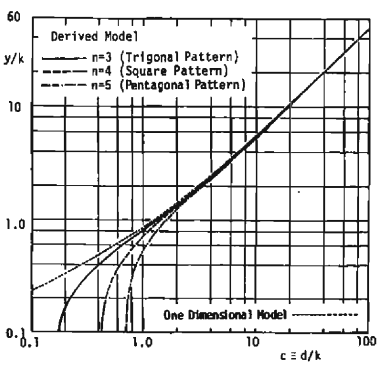

Fig. D Height of Particles Resting on Basic Rough Beds.

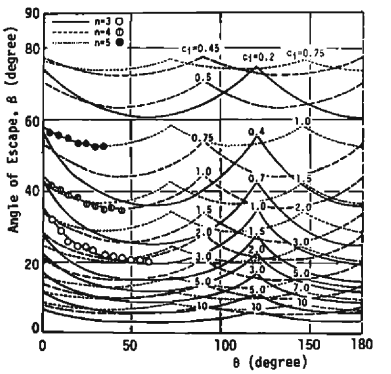

Fig. E Angle of Escape.

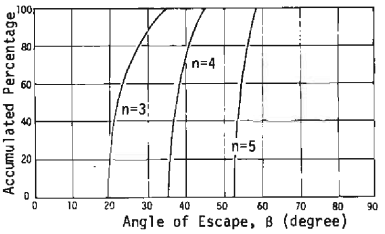

Fig. F Distribution of Angle of Escape for Each Basic Pattern.

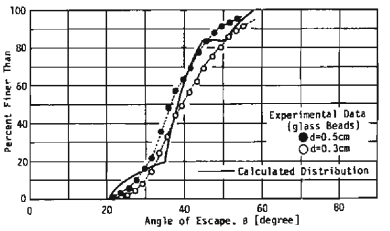

Fig. G Distribution of Angle of Escape (Spherical Uniform Particles).

Using the above values for f_n and **Fig. F**, a semi-theoretical curve can be drawn on **Fig. G**, which is indicated by a solid line. According to the above consideration, the average value of angle of escape for uniform particle is about 36°～40° and it is larger than that obtained in the section **2.3** by one-dimensional model. Additionally, for the case of actual sand bed, this value may be further larger due to the geometry of actual sand.

Appendix B—Equivalent Sand Roughness of Artificial Roughness

In the section **3.3** of this paper, a new method to determine the equivalent sand roughness of rough bed composed of sand mixture has been proposed, and this model will be here applied to artificial two-dimensional roughness, which is illustrated in **Fig. H**. The symbols K, b and t are defined as shown in **Fig. H**.

Applying the idea on the equivalent size, as mentioned in section **3.3** of this paper, to this case, the equivalent sand roughness $k_s=\alpha d_e$ can be obtained by solving the following equation:

$$\frac{\varepsilon_0}{2}C_D\rho u_{b0}^2 A_2 d_e^2 \frac{1}{A_2 d_e^2}=\frac{\varepsilon_A}{2}C_{DA}\rho u_{bA}^2(K-y_b)\frac{1}{b+t}. \tag{h}$$

where the subscript A represents the value with respect to artificial roughness element, and y_b is the height of the theoretical wall from the lowest bed surface. The theoretical wall is here assumed to be defined as the plane beneath which the volume equals that of the upper layer of the roughness elements, as suggested for the case of the clossly-packed hexagonal arrangement of hemispheres by Bennedict et al.[b] Then,

$$y_b=Kt/(B+t) \tag{i}$$

If the local velocity u_{bA} is assumed to be that at the height $a_A(K-y_b)$ given by the logarithmic law, k_s is obtained as follows.

$$k_s/K=30.1a_A(1-y_b/K)/(30.1a/\alpha)^{1/B} \tag{j}$$

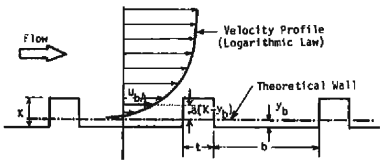

Fig. H Two-Dimensional Artificial Roughness.

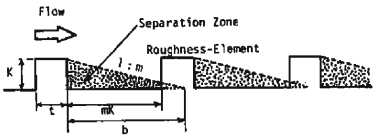

Fig. I Serarated Zone of Flow in Downstream of Roughness Element.

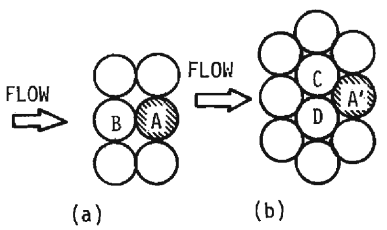

Fig. J Idealized Sand Bed.

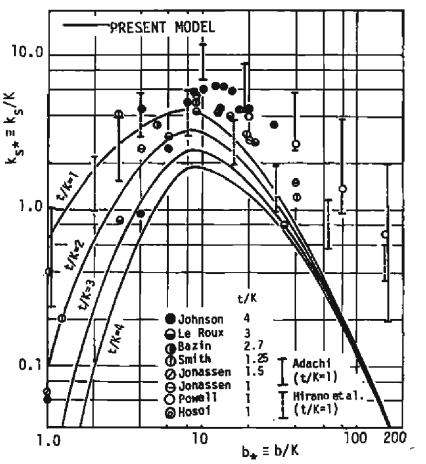

Fig. K Equivalent Sand Roughness of Two-Dimensional Artificial Roughness.

where

$$B^2 = (\varepsilon_A C_{DA}/\varepsilon_0 C_D) \cdot \{Kb/(b+t)^2\} \qquad (k)$$

Though ε_i and C_{Di} have been assumed to be identical irrespectively of sand diameter in case of sand mixture, ε_A and C_{DA} in this case must be quite different from ε_0 and C_D respectively. It is assumed that $C_{DA}=1.0$ according to the experiment by Hirano et al.,[c] where the representative velocity for drag coefficient has been regarded as the velocity at the top of the roughness element and then $a_A=1.0$. On the other hand, the sheltering effect is considered by a simplified model as explained below. In the case of artificial roughness element shown in **Fig. H**, the separation zone of flow in the downstream of a roughness element may be assumed as illustrated in **Fig. I.** The length of such a separation zone is experimentally known to be about 7～8 times the roughness height, and then, ε_A is assumed to be expressed by

$$\varepsilon_A = \begin{cases} (1/m) \cdot (b/K) & (b/K \leqq m) \\ 1.0 & (b/K > m) \end{cases} \qquad (l)$$

where $m=7\sim8$. Though the above estimation is too rough, it is the ratio of the sheltering coefficients to be considered, and then, ε_0 should be obtained by

the similar way. For simplicity, idealized conditions as shown in **Fig. J** are considered, where particle A or A' is the main particle. This particle A or A' is to be sheltered by only the particle B or the particles C and D, respectively. Considering the decrease of the projected area for flow of the particle A or A' and that ε_0 can be obtained by the similar way to the above discussion; $\varepsilon_0=0.321$ or 0.278, respectively for A and A'. Therefore, the average value of ε_0 may be determined as 0.30. Consequently, the relationship between $k_{s*}\equiv k_s/K$ and $b_*\equiv b/K$ can be estimated with a parameter $t_*\equiv t/K$ as shown in **Fig. K**. On calculation, it is assumed that $a_A=1.0$, $\alpha=3.0$, $m=8.0$ and $\varepsilon=0.30$. In **Fig. K**, the experimental data collected by Johnson,[d] Powell,[e] Adachi[f] and Hirano et al.[c] are also shown. According to this figure, the equivalent sand roughness is underestimated appreciably in the case where b_* is large. The reason for this tendency is that the skin friction is not considered in the present model, but this effect is dominant when the number density of roughness elements is small. Considering this effect, the experimental data may be explained well by the method derived in this appendix.

---

a) Nakagawa, H. and T. Tsujimoto: Study on Mechanism of Motion of Individual Sediment Particles. Proc. JSCE, No. 244, pp. 71–80, 1975, (in Japanese).

b) Benedict, B. A. and B. A. Christensen: Hydrodynamic Lift on a Stream Bed. Proc. Sedimentation Symposium to Honor Prof. H. A. Einstein, Berkeley, California, USA, Chapter 5, 17p., 1971.

c) Hirono, M. and K. Iwamoto: Resistance and Mean Velocity of Flow on Large Scale Roughness. Shin-Sabo (Journal of the Erosion Control Engineering Society, Japan), No. 110, pp. 8–13, 1979, (in Japanese).

d) Johnson, J. W.: Rectangular Artificial Roughness in Open Channels. Trans. A.G.U., Hydrology Section, pp. 909–914, 1944.

e) Powell, R. W.: Flow in a Channel of Definite Roughness. Trans. ASCE, Vol. 111, pp. 531–566, 1944.

f) Adachi, S.: Experimental Study on Artificial Roughness. Trans. JSCE, No. 104, pp. 33–44, 1964, (in Japanese).